PROCEEDINGS OF SCIENCE

Impact of Galaxy Clusters on UHECR propagation

Antonio Condorelli,[a,*] **Jonathan Biteau**[a] **and Remi Adam**[b]

[a] *Université Paris-Saclay, CNRS/IN2P3, IJCLab, 15 Rue Georges Clemenceau, 91405 Orsay, France*
[b] *Université Côte d'Azur, Observatoire de la Côte d'Azur, CNRS, Laboratoire Lagrange, France*

E-mail: condorelli@ijclab.in2p3.fr

Galaxy clusters are the largest objects in the universe that are held together by their own gravity. Most of their baryonic content is made of a magnetized diffuse plasma. We investigate the impact of such a magnetized environment on ultra-high-energy cosmic-ray (UHECR) propagation. The intracluster medium is described according to the self-similar assumption, in which the gas-density and pressure profiles are fully determined by the mass and redshift of the cluster. The magnetic field is scaled to the thermal components of the intracluster medium under different assumptions. We model the interactive and diffusive processes of UHECRs in the intercluster medium using a modified version of the Monte Carlo code *SimProp*, where hadronic processes and magnetic confinement are implemented, as well as the effect of the cluster's magnetic field. We provide a universal parametrization of the UHECR flux escaping from the environment as a function of the most relevant quantities, such as the mass of the cluster, the position of the source with respect to the center of the cluster and the nature of the accelerated particles. We show that galaxy clusters are an opaque environment, especially for UHECR nuclei. The role of the most massive nearby clusters in the context of the emerging UHECR astronomy is finally discussed.

38th International Cosmic Ray Conference (ICRC2023)
26 July - 3 August, 2023
Nagoya, Japan

*Speaker

PoS(ICRC2023)335

1. Introduction

The origin of cosmic rays at the highest energies remains a mystery, despite the fact that they have been observed for more than a century. We have been able to examine their spectral behavior and atomic mass composition on Earth thanks to observations, but the astrophysical sources of ultra-high-energy cosmic rays (UHECRs), i.e. cosmic rays exceeding 10^{18}eV, are still unknown [1, 2].

Astrophysical accelerators to ultra-high energies are expected to be distributed following the baryonic matter along the cosmic web. Galaxy clusters are the most massive virialized structures of the cosmic web, with typical radii of $R_{\rm cl} = 1 - 2\,$Mpc and total masses of $M \simeq 10^{14} - 10^{15} M_{\odot}$, which include both baryonic and dark matter. Clusters have powerful turbulent magnetic fields with root mean square values of $B \simeq$ few μG. This suggests that cosmic rays that have been accelerated in cluster candidate sources or in accretion shocks may be long-term confined.

Clusters may host or cast a shadow over some of the extragalactic sources of UHECRs. In the sections that follow, we assess whether UHECRs are capable of leaving these types of environments and how clusters should be taken into account in UHECR astronomy. We propose a single parametrization of the escaping flux that is dependent on the cluster mass as well as on UHECR properties such as energy and atomic mass.

2. Intracluster medium modeling

Clusters of galaxies and the filaments that connect them are the biggest structures in the current universe, where the gravitational force owing to matter over-density exceeds the expansion of the cosmos. Massive clusters typically have total masses of $10^{14} - 10^{15} M_{\odot}$, with dark matter making up the majority of that mass ($70 - 80\,\%$ of the total mass). By contrast, galaxies make up a small percentage of the total mass while baryonic matter makes up the hot ($T \simeq 10^{8}\,$K) and tenuous ($n_{\rm gas} \simeq 10^{-1} - 10^{-4}\,{\rm cm}^{-3}$) gas ($15 - 20\,\%$) that forms the intracluster medium (ICM) [3]. Measurements of the gas-density profile, magnetic field profile, and coherence length are required to predict UHECR propagation in clusters. While the magnetic field clusters is constrained by a restricted amount of data, some of which are model-dependent, the gas density is well understood and frequently obtained from X-ray observations. Fortunately the magnetic-field intensity is inferred to scale with the ICM thermal density or pressure.

Galaxy clusters have an intriguing characteristic of being self-similar objects at first order, which allows their physical features to be fully defined given their mass and redshift [4]. For example, their universal pressure profiles (UPP) and universal density profiles (UDP) are currently well defined from observations [5]. Following [6], we use the UPP expressed as

$$P(x) = \frac{P_0 \times P_{500}(M_{500}, z) \times f(M_{500}, z)}{(c_{500}x)^{\gamma_{\rm p}} \cdot (1 + (c_{500}x)^{\alpha_{\rm p}})^{\frac{\beta_{\rm p}-\gamma_{\rm p}}{\alpha_{\rm p}}}}, \tag{1}$$

with $P_{500}(M_{500}, z)$ the self-similar normalization [7], $f(M_{500}, z)$ the mass-dependence correction, while P_0, c_{500}, $\alpha_{\rm p}$, $\beta_{\rm p}$, $\gamma_{\rm p}$ are parameters that describe the shape of the profile as a function of the scaled radius $x = r/R_{500}$. The mass M_{500} is defined within R_{500}, the radius within which the cluster density is 500 times the critical density of the universe at the cluster redshift.

Similarly, we use the UDP as measured by [5], which can be expressed as

$$n(x) = \frac{A(M_{500}, z) \times f_0}{(x/x_s)\,(1 + (x/x_s)^{\gamma_d})^{\frac{3\beta_d - \alpha_d}{\gamma_d}}}. \tag{2}$$

The quantity $A(M_{500}, z)$ describes the normalization as a function of mass and redshift, and the parameters $f_0, x_s, \alpha_d, \beta_d, \gamma_d$ describe the shape.

By scaling through the mean molecular weights with the gas density, we can determine the electron-, proton-, and helium-density profiles. The proton density profile of the Coma cluster, is shown in the left panel of Figure 1, where it is compared to the model derived from our methodology, using the mass and redshift from the MCXC catalog [8]. Our reference model, which was constructed by combining the UPP profile and the polytropic relation, is represented by the green line. The UDP profile, calibrated by [5] and [9], is shown in red and purple, respectively, for further comparison.

The profile of magnetic-field strength can be scaled to the thermal-gas density, under the assumption that the thermal energy is proportional to the magnetic energy density:

$$\langle B^2(r) \rangle = 2\mu_0 P(r)/\beta_{\rm pl}, \tag{3}$$

with μ_0 the vacuum permeability. For the plasma, we set $\beta_{\rm pl} = 200$ following the results by [10] on the Perseus cluster. Alternatively, assuming that the magnetic field is frozen into the plasma and amplifies under pure adiabatic compression with magnetic flux conservation, we have

$$\langle B^2(r) \rangle = B^2_{\rm ref} \left(\frac{n_{\rm gas}(r)}{n_{\rm gas}(r_{\rm ref})} \right)^{4/3}. \tag{4}$$

The normalization $B_{\rm ref}$, taken at the radius $r_{\rm ref}$, is defined using the reference Coma cluster, for which comprehensive measurements are provided in [11].

In Figure 1, we compare the magnetic-field profile of the Coma cluster estimated from Faraday rotation measures [11] to our models. The green line gives the profile estimated using Equation 3, with $\beta_{\rm pl} = 200$, combined with the UPP from [6]. The purple line is based instead on $\beta_{\rm pl} = 77$, following Plank measurements on Coma cluster [12]. The red line uses Equation 4 with the density estimated from the UDP calibrated by [13]. We see that, despite the fact that our modeling is based on some very strong assumptions, the prediction and measurement generally agree within a factor 1.4. This is also true in the inner region of the cluster, where, we show that in Sec. 3, UHECR propagation is predicted to be significantly influenced by the environment.

3. UHECR propagation in galaxy clusters

3.1 Interactions and diffusion in a cluster

We use a modified version of the Monte Carlo tool *SimProp* [14] to calculate the typical timescales for photo-hadronic and hadronic interactions of UHECRs in the cluster environment. We take into consideration hadronic interactions in the ICM as well as interactions with photons from the cosmic microwave and infrared backgrounds.

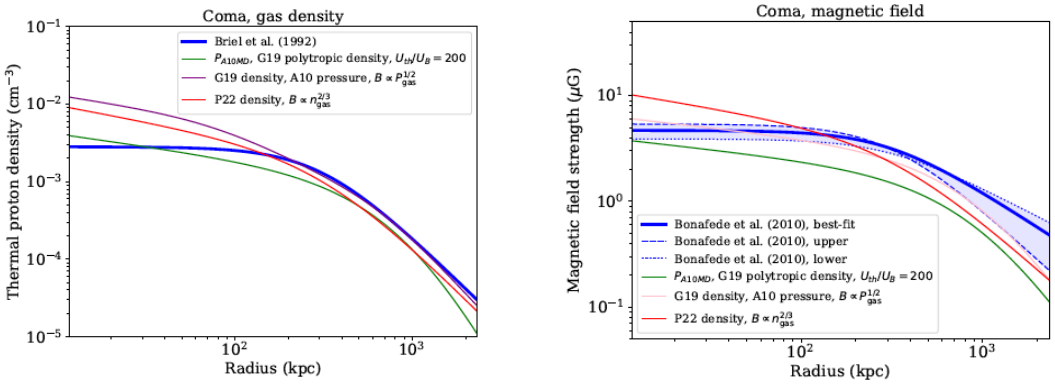

Figure 1: Left panel: Thermal proton density profiles for the Coma cluster. Right panel: Magnetic field strength profiles for Coma cluster.

The typical interaction rate between a relativistic atomic nucleus (A) and a low-energy photon, under the assumption of a monochromatic photon field of number density n_γ, is roughly $\tau_{A\gamma}^{-1} \simeq c\sigma_{A\gamma} n_\gamma$, where $\sigma_{A\gamma}$ represents the cross section of the process and c is the speed of light in vacuum. When the dependence of the cross section on energy and a more realistic spectral energy distribution for the photon field are taken into consideration, the interaction rate is as follows [15]:

$$\frac{dN_{\rm int}}{dt} = \frac{c}{2\Gamma} \int_{\epsilon'_{\rm th}}^{\infty} \sigma_{A\gamma}(\epsilon')\epsilon' \int_{\epsilon'/2\Gamma}^{\infty} \frac{n_\gamma(\epsilon)}{\epsilon^2}\, d\epsilon\, d\epsilon', \tag{5}$$

where Γ is the Lorentz factor of the interacting nucleus. Spallation between UHECRs and gas has minimal impact in the extragalactic medium, however because of the effective time that relativistic particles spend in the ICM, their influence can be significant. The timescale of the spallation process is as follows:

$$\tau_{\rm spal} = n_{\rm ICM}\, \sigma_{\rm sp}\, c^{-1}, \tag{6}$$

where $n_{\rm ICM}$ is the ICM gas density and $\sigma_{\rm sp}$ is the cross section for proton-proton or proton-nucleus interactions.

In addition to interactions, diffusion in the magnetic field has to be taken into account. The diffusion timescale reads: $t_{\rm D} = R^2/D$, where R is the radius of the environment and D is the estimated cosmic-ray diffusion coefficient in the framework of quasi-linear theory under the assumption of Kolmogorov turbulence and a coherence length $l_c \sim 1$ pc for the magnetic field. The expression of the diffusion coefficient is $D = r_L^{1/3} l_c^{2/3}/3$, where r_L is the particle Larmor radius. In agreement with [16], we also take into account the change in the diffusion regime that occurs when $r_L \gtrsim l_c$. The particle moves ballistically at the highest energies, leading to the diffusion time approaching R/c. The typical length-scales for interactions and escape in the source environment for a prototype cluster are presented in Figure (2) (see caption). Both the nuclear composition at the cluster escape and the shape of the UHECR fluxes are controlled by the interplay between length scales. Diffusion always determines the smallest length-scale for protons, which indicates that some of the protons may be able to escape. The photo-interaction times for nuclei (such as nitrogen in Figure 2) are the shortest at high rigidities for the selected cluster parameters (see caption).

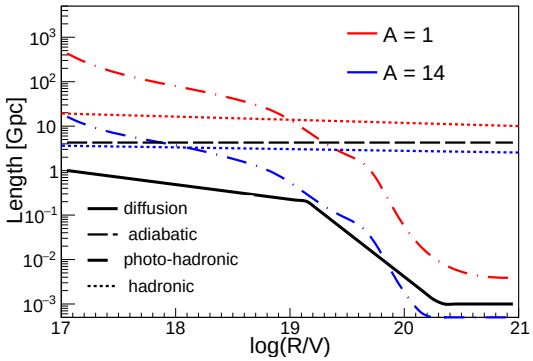

Figure 2: Interaction and escaping lengths as a function of magnetic rigidity at the center of a prototypical galaxy cluster: photo-hadronic interaction times (dashed-dot lines), spallation times (dashed lines) and diffusion times (solid lines) for protons (red) and nitrogen nuclei (blue). The Hubble radius (corresponding to the age of the universe) is shown as a long-dashed line. Length scales have been calculated assuming the following parameters: $R_{500} = 1$ Mpc, $B = 1$ μG, $l_c = 10$ kpc, $n_{\rm ICM} = 1 \cdot 10^{-4}$ cm^{-3}.

4. UHECR flux escaping the ICM

Once the particles have escaped from the magnetic environment, the impact of the ICM on the UHECR spectrum may be calculated as a function of the injection position. We inject 10^4 particles with logarithmic distribution in the energy range $10^{17} - 10^{21}$ eV.

In order to explain the escaping fluxes above the ankle, we present a parametrization of the escaping fluxes as a function of the mass of the cluster M, the position of the injection point y, and the nature of the accelerated particles (protons or nuclei) based on the simulations. Four representative nuclear masses are investigated: ^{1}H, ^{4}He, ^{14}N, ^{28}Si. The contribution of iron nuclei is ignored since it is assumed to be small from simple cosmological models that describe data from the Pierre Auger Observatory [17, 18].

Based on the simulations, we model clusters as transparent for accelerators placed at $y > 0$, i.e. between the cluster's center and the observer, and we provide a single parametrization of cluster transparency for $y \leq 0$, i.e. behind the cluster's center. We define a cluster's transparency $f(R)$ as the escaping flux divided by the one expected without interactions in the ICM and considering only ballistic propagation. We use a broken power-law to approximate transparency as a function of rigidity R, with full transparency at the highest energies:

$$\log\ f(R) = \begin{cases} 1 + \Gamma\ \log(R/\rho) & R \leq \rho, \\ 1 & R \geq \rho. \end{cases} \tag{7}$$

We notice that the break rigidity, ρ, depends on the mass of the cluster, M, following to first order:

$$\log \rho = \log \rho_0 + \xi \log(M/10^{15} M_{\odot}). \tag{8}$$

We parameterize the low-rigidity slope, Γ of the transparency function, so that it reaches a maximum value of 2 at high cluster masses and softens at lower masses:

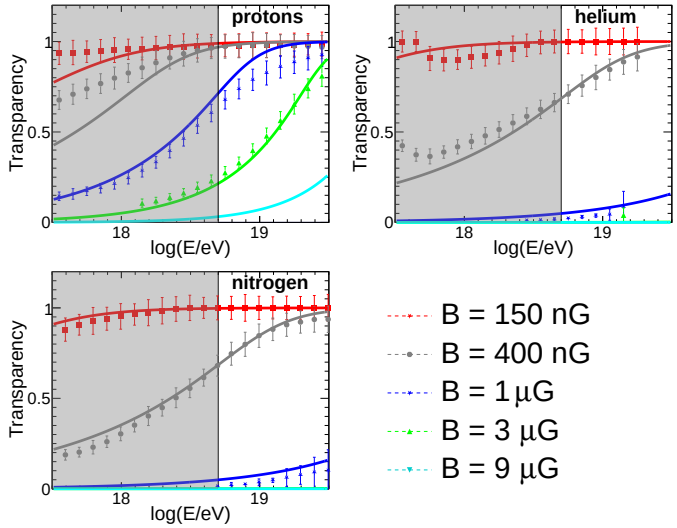

Figure 3: Transparency as a function of energy for protons, helium and nitrogen nuclei for different cluster magnetic field (see legend), assuming an an injection point at the center of the environment. The points show the results obtained from the simulations with errors resulting from the number of injected particles. The solid lines display the proposed parametrization. The vertical line shows the ankle energy.

$$\Gamma = \frac{2}{1 + \left(\frac{M}{M_{\text{free}}}\right)^{-\sigma}}. \tag{9}$$

We find that $\log(M_{\text{free}}/M_{\odot}) = 14.4 \pm 0.5$ is consistent with the transparency functions of both nuclei and protons. The parameter σ determines the evolution of the index with cluster mass. In this situation, we also find a shared value $sigma = 0.25 \pm 0.10$ for nuclei and protons.

The parameters are obtained by fitting the model in Equation 7 to the escape fluxes for various positions of the sources at $y \leq 0$ and for various cluster masses, taking either protons or nuclei into account. We find that the best parameter values for protons are $\log(\rho_0/\text{V}) = 20.0 \pm 0.2$ and $\log(\rho_0/\text{V}) = 24.3 \pm 0.3$ for nuclei, whereas $\xi = 0.6 \pm 0.1$ for protons and $\xi = 1.7 \pm 0.2$ for nuclei. Figure 3 shows a comparison to simulated data for an injection at the cluster's center.

For nuclei, the two parameters that impact the rigidity at which the transition occurs, ρ_0 and xi, are higher for nuclei than for protons. This is because nuclei interact more than protons in the ICM, as shown in Figure 2; as a result, the transition to $f(R) = 1$ occurs at higher rigidities for nuclei.

According to our models, clusters of mass $M = 10^{14} M_{\odot}$ or $M = 10^{15} M_{\odot}$ with central magnetic fields of 3 and 9 μG, respectively, can trap almost all protons up to the ankle. Above the ankle, the effect of the ICM on protons is insignificant for lower magnetic fields. Similar conclusions can be derived for nuclei; however, it is crucial to note that for clusters with central magnetic fields greater than 1 μG, they are totally disintegrated up to at least the ankle. The proposed parametrization accurately represents the effect of the galaxy cluster on the escaping fluxes above the ankle. The approximation of assuming the environment as transparent for sources with $y > 0$ describes well

the simulations findings for weakly magnetized clusters. The proposed parametrization for $y > 0$ overestimates the escape fluxes on average by 0.4 dex for clusters with $B \geq 3\ \mu$G.

Overall, we conclude that only a small fraction of nuclei can escape from clusters with central magnetic field of $B \geq 1\ \mu$G up to energies of 10^{19} eV for He and $10^{19.5}$ eV for N. Protons are also highly suppressed in the most massive clusters: only 40% escape at 10^{19} eV for a central magnetic field of 3 μG, whereas almost none escape at this energy for $B \geq 9\ \mu$G. As a result, galaxy clusters are hostile environments for UHECRs. The filtering is stronger for nuclei, which are entirely disintegrated in the most massive clusters, even in the most remote parts of the environment.

5. Discussion

For this work, we work under the assumption of self-similarity of cluster properties. Given the mass and redshift of the clusters, it is possible to derive the crucial quantities for UHECR propagation, namely the magnetic-field and gas density profiles. The cluster environment works as a high-pass filter as a function of rigidity, allowing some UHE protons to escape while the UHE nuclei interact with the gas and photons in the ICM.

The current work leads to important findings for the growing field of UHECRs astronomy: we should not observe UHE nuclei from massive galaxy clusters above the ankle energy based on our calculations. This includes the Virgo cluster, the nearest galaxy cluster to us ($d \simeq 16$ Mpc, $M \simeq 1.2 \cdot 10^{14}\ M_{\odot}$). Assuming that the UHECR production rate follows the rate of star formation or stellar mass of nearly half a million galaxies, [19] observed that the computed skymaps should show an excess in the direction of the Virgo cluster, which is not evident in the measured skymaps [20]. Our results demonstrate that magnetic trapping of UHECRs in Virgo lowers this tension, as previously proposed in [21]. The results of our work not only decrease the inconsistencies between the arrival direction model and the data, justifying the lack of UHE nuclei in the directions of the galaxy clusters, but they also offer fascinating pathways for further research into composition anisotropies, as only protons could escape from these environments.

Another application of our research is the dipole seen by the Pierre Auger Observatory above 8 EeV, the direction of which is qualitatively described by the distribution of local extragalactic matter and UHECR deflections in the Galactic magnetic field [22]. The substantial contribution to the dipole from the Virgo cluster inferred, for example, by [23] should be significantly reduced when magnetic trapping and shadowing in the ICM are taken into consideration. This is also true for the Perseus cluster ($d \simeq 74$ Mpc, $M \simeq 5.8 \cdot 10^{14}\ M_{\odot}$), for which the Telescope Array collaboration asserts an indication of excess at energies exceeding $5.7 \cdot 10^{19}$ eV [24]. Our work tends to rule out the possibility that the Telescope Array and the Pierre Auger Observatory see UHE nuclei accelerated by a host source close to the center of the Perseus or Virgo clusters; either they must come from off-centered galaxies or they must be UHE protons, both primary and secondary due to heavy nuclei fragmentation in the environment surrounding the accelerator.

6. Aknowdlegements

AC and JB gratefully acknowledge funding from ANR, via the grant MultI-messenger probe of Cosmic Ray Origins (MICRO), ANR-20-CE92-0052.

References

[1] Abreu, P. et al., *Phys. Rev. Lett.*. **130**, 061001 (2023,2)

[2] Abreu, P. et al., *The Astrophysical Journal*. **933**, 125 (2022,7)

[3] Voit, G. *Reviews Of Modern Physics*. **77**, 207-258 (2005,4)

[4] Kaiser, N. MNRAS **222** pp. 323-345 (1986,9)

[5] Pratt, G., Arnaud, M., Maughan, B. & Melin, J. *Astron. Astrophys.*. **665** pp. A24 (2022), [Erratum: Astron.Astrophys. 669, C2 (2023)]

[6] Arnaud, M., Pratt, G., Piffaretti, R., Böhringer, H., Croston, J. & Pointecouteau, E. *A& A*. **517** pp. eA92 (2010,7)

[7] Nagai, D., Kravtsov, A. & Vikhlinin, A., *Astrophysical Journal* **668**, 1-14 (2007,10)

[8] Piffaretti, R., Arnaud, M., Pratt, G., Pointecouteau, E. & Melin, J. *A& A*. **534** pp. eA109 (2011,10)

[9] Ghirardini, V. et al., *A& A*. **621** pp. A41 (2019,1)

[10] Walker, S. et al., *MNRAS*. **468**, 2506-2516 (2017,6)

[11] Bonafede, A. et al., *A& A*. **513** pp. A30 (2010,4)

[12] Planck Collaboration, *A & A*. **554** pp. eA140 (2013,6)

[13] Pratt, G., Croston, J., Arnaud, M. & Böhringer, H. *A& A*. **498**, 361-378 (2009,5)

[14] Aloisio, R., Boncioli, D., Grillo, A., Petrera, S. & Salamida, *Journal Of Cosmology And Astroparticle Physics*. **2012**, 007-007 (2012,10)

[15] Aloisio, R., Berezinsky, V. & Grigorieva, S. *Astroparticle Physics*. **41** pp. 73-93 (2013,1)

[16] Subedi, P. *The Astrophysical Journal*. **837** pp. 140-150 (2017)

[17] Luce, Q., Marafico, S., Biteau, J., Condorelli, A. & Deligny, O. *The Astrophysical Journal*. **936**, 62 (2022,8)

[18] Abdul Halim, A. et al., *JCAP* **5** pp. 024 (2023)

[19] Biteau, J. *The Astrophysical Journal Supplement Series*. **256**, 15 (2021,9)

[20] Abreu, P. et al., *The Astrophysical Journal*. **935**, 170 (2022,8)

[21] Biteau, J., Marafico, S., Kerfis, Y. & Deligny, O, PoS ICRC2021 **1012** (Preprint 2108.10775)

[22] Aab, A. et al., *Science* **357**, 1266-1270 (2017)

[23] Ding, C., Globus, N. & Farrar, G. *The Astrophysical Journal Letters*. **913**, L13 (2021,5)

[24] Telescope Array Collaboration, *ArXiv E-prints*. earXiv:2110.14827 (2021,10)